applied sciences

MDPI

Article

Emission Behaviors of Inorganic Ultrafine Particles during Zhundong Coal Oxy-Fuel Combustion with Characterized Oxygen Input Fractions Comparable to Air Combustion

Bin Fan [1,2], Chang Wen [1,3,*], Xianpeng Zeng [1], Jianqun Wu [1] and Xin Yu [1]

1 State Key Laboratory of Coal Combustion, School of Energy and Power Engineering, Huazhong University of Science and Technology, Wuhan 430074, China; fanbingreen@163.com (B.F.); X.P_Zeng@foxmail.com (X.Z.); wujianqun1988@hust.edu.cn (J.W.); hustyuxin@hust.edu.cn (X.Y.)
2 School of Materials Science and Engineering, Jingdezhen Ceramic Institute, Jingdezhen 333403, China
3 Department of New Energy Science and Engineering, School of Energy and Power Engineering, Huazhong University of Science and Technology, Wuhan 430074, China
* Correspondence: wenchang@hust.edu.cn; Tel.: +86-27-8754-4779

Received: 27 July 2018; Accepted: 23 August 2018; Published: 29 August 2018

Abstract: Zhundong low-rank coal is very likely to be utilized extensively in oxy-fired boilers in the near future. Its PM_{10} (particulate matter with an aerodynamic diameter of $\leq$10 μm) emission behaviors during oxy-fuel combustion need to be carefully studied before its large-scale use. The present study examines the emission behaviors of inorganic ultrafine particles ($PM_{0.5}$, with an aerodynamic diameter of $\leq$0.5 μm), as well as PM_{10} during the combustion of Zhundong coal in air and oxy-fuel conditions (O_2/CO_2) at three characterized O_2 input fractions, i.e., 21, 27 and 32 vol.%. The combustion experiments were carried out in a high-temperature drop-tube furnace (HDTF) at a combustion temperature of 1500 °C. The results show that $PM_{0.5}$ is composed of Na, S, Mg and Ca, with total fractions of ~90%, while $PM_{0.5–10}$ (with an aerodynamic diameter between 0.5 and 10 μm) predominantly contains Ca (~50–65%). At three characterized oxygen fractions during oxy-fuel combustion (OXY21, 27 and 32), the promoted O_2 fraction was found to increase the yields of both $PM_{0.5}$ and $PM_{0.5–10}$. A higher particle-burning temperature and a lower CO_2 fraction promote the reactions of both organically bound elements and inorganic minerals, increasing the partitioning of Mg and Ca and causing an increased yield of $PM_{0.5}$. The yield of $PM_{0.5}$ from air is high and similar to that from OXY32 while the yield of $PM_{0.5–10}$ from air is similar to that from OXY27. The high yield of $PM_{0.5}$ from air is mainly generated by the highest yields of Ca in four conditions.

Keywords: Zhundong coal; oxy-fuel combustion; characterized oxygen fraction; particulate matter; high temperature

1. Introduction

Coal is still one of the most important energy resources in China; it accounts for ~62% of the total energy demand nowadays and causes many environmental problems such as SOx, NOx, PM (particulate matter) and heavy metals [1–6]. The newly discovered Zhundong coal field is the largest intact coalfield with a predicted reserve of ~390 billion tons, located in Junggar Basin in the Xinjiang Autonomous Region of China. Zhundong coal was reported to show the typical combustion characteristics of a low-rank coal [7,8], i.e., it consisted of sequential and overlapping stages of volatile release and char combustion [9,10]. To better utilize it in a power boiler, Chinese researchers have paid attention to the obvious ash deposition problems, such as slagging, fouling and corrosion, which are mainly caused

by the high sodium and calcium content of Zhundong low-rank coal [11–16]. However, the emission of PM during Zhundong coal combustion, also as an important ash-related problem, has rarely been reported until now. The distinctive coal was reported to emit much more PM_{10} (particulate matter with an aerodynamic diameter of $\leq$10 μm) than other lignite and bituminous coals during combustion [12], which could cause both the operating problem of initial deposition and the environmental problem of haze [17].

Oxy-fuel (O_2/CO_2) combustion was proposed as a retrofit technology to allow for the capture and storage of CO_2 in new or existing air-fired coal boilers [18–20]. Recently, it reached a milestone 35 MW load [21]. In the near future, Zhundong low-rank coal is very likely to be utilized extensively in oxy-fired boilers, therefore the PM emission behaviors of Zhundong coal during oxy-fuel combustion need to be carefully studied before its large-scale use. As CO_2 replaces N_2 to dilute O_2 in oxy-fuel technology, the furnace temperature and heat transfer differ from those in air combustion because of the higher thermal capacity of CO_2 and the lower diffusivity of O_2 in CO_2 [22]. A higher initial O_2 fraction should be necessary to achieve a similar furnace temperature to air combustion. Morris et al. reported that an O_2 fraction of 27% was calculated to match the radiant heat flux of the flue gas in air-fired combustion, and a fraction of 32% matched the adiabatic flame temperature [23,24]. Therefore, the principal purpose of this study is to examine the possible difference in PM emission behaviors of Zhundong coal during oxy-fuel combustion in the three characterized O_2 input fractions comparable to air combustion, i.e., 21%, 27% and 32 vol.% of O_2 in a O_2/CO_2 mixture.

Table 1. Studies on the effect of O_2 fraction on the emission behaviors of particulate matter (PM) during oxy-fuel coal combustion.

Coal Type	Furnace Temperature	O_2 Fractions in O_2/CO_2 Combustion	Results as the Increase of O_2 Fraction	References
PRB sub-bit [1]	1200 °C	20, 25, 40, 50%, versus air	Geometric mean size of the submicron particles (PM_1) increased because the higher particle surface temperature of the coal resulted in faster mineral vaporization rates.	Suriyawong et al. [25]
Three Chinese bituminous coals	1400 °C	20, 40%, versus air	Promoted impacts on the formation of fine ash particles in both the submicron mode and the fine fragmentation mode.	Sheng et al. [26,27]
PSOC-1451 sub-bit, DECS-26 bit [2], PSOC-1443 lignite	1127 °C	30, 40, 60%, versus air	Submicrometer particle emission yields increase and the composition of the ultrafine PM was affected; submicrometer ash yields of lower rank coals were more affected; no clear trend for the fine fragmentation mode.	Kazanc et al. [28,29]
Utah bit, Illinois bit, PRB sub-bit	1137 °C, 1247 °C	21, 31.5%, versus air	Diameter and mass for the coarse particles did not change, while those for $PM_{0.1}$ increased.	Jia et al. [30]
Utah bit, Illinois bit, PRB sub-bit	<1100 °C	21, 27, 32%, versus air	Nucleation modes for the Utah and PRB coals were shown to consist of significant amounts of soot; no clear trend for the central mode (i.e., fine fragmentation mode).	Morris et al. [24] Yu et al. [23]

[1] sub-bit: sub-bituminous coal; [2] bit: bituminous coal.

The effect of O_2 fractions on PM emissions during oxy-fuel coal combustion has been reported by several researchers, and some notable information can be found in the summary presented in Table 1. Firstly, studies on low-rank coals chose a furnace temperature of <1200 °C, which is much lower than that of the existing utility boiler (~1400–1600 °C). During coal combustion, a lower burning temperature would inhibit the vaporization of inorganic matters and the fragmentation of char particles [31], and even bring in the soot into ultrafine particles as a result of incomplete combustion, all of which would obviously affect the emission of inorganic PM. Moreover, most studies paid attention to O_2 fractions much higher than 30%; the above-mentioned three characterized O_2 fractions comparable

to the air atmosphere were only studied by Morris et al. [24] in a down-fired oxy-fuel combustor. However, in their study the ultrafine particles consisted mostly of undesired soot, which may have been caused by the low furnace temperature (<1100 °C). Beyond this, different coal types have varied ash compositions, which also affect the emission of inorganic PM. As such, the principal purpose of our research, i.e., to clarify the emission behaviors of inorganic PM during the oxy-fuel combustion of Zhundong coal before its possible large-scale use cannot be assessed on the basis of other related publications and requires careful research.

In this study, a similar combustion temperature (1500 °C) to a utility boiler was chosen in a high-temperature drop-tube furnace (HDTF, RHTV 120-600/18, Nabertherm, Lilienthal, Bremen, Germany) to ensure the complete combustion of Zhundong coal, and three characterized O_2 fractions (21, 27 and 32 vol.%) in O_2/CO_2 combustion were used to achieve the same oxygen content, a similar heat transfer flux and a similar adiabatic flame temperature to air combustion, respectively. Mass-based particle size distributions (PSDs), mass yields and chemical compositions of inorganic PM were carefully analyzed to clarify the emission behaviors of the ultrafine particles and PM_{10} generated from the combustion of the giant Chinese power coal.

2. Materials and Methods

2.1. Coal Properties

A typical Zhundong coal had been used in earlier research [16,32], which was crushed, ground and sieved to obtain a narrow-sized coal sample in a range of 63–100 μm. The proximate and ultimate analysis and the inorganic compositions of the Zhundong coal sample are shown in Table 2. It is a low-ash and low-sulfur coal which can be classified as a sub-bituminous coal. The results of the XRF (X-ray Fluorescence, EDAX EAGLE III, EDAX Inc., Mahwah, NJ, USA) analysis on low-temperature ash for coal show an abundance of Ca, S, Na and Mg.

Table 2. Proximate, ultimate and ash composition analysis of Zhundong coal.

	Proximate analysis (wt %, air-dried)				*Ultimate analysis (wt %, air-dried)*				
Zhundong Coal	M [1]	A [2]	VM [3]	FC [4]	C	H	O [5]	N	S
	7.25	3.56	40.13	49.06	65.77	3.95	14.60	4.36	0.51
	Chemical composition analysis of low-temperature ashes (wt %)								
Zhundong Coal	Na_2O	K_2O	SO_3		CaO	Fe_2O_3	MgO	Al_2O_3	SiO_2
	4.30	0.51	26.92		37.96	3.89	10.66	8.76	7.00

[1] Moisture; [2] Ash; [3] Volatile matter; [4] Fixed carbon; [5] Counted by difference.

To distinguish between the occurrence forms of major inorganic elements, the coal was sequentially extracted with deionized water, 1 M ammonium acetate (CH_3COONH_4, NH_4OAc), 1 M hydrochloric acid (HCl) at a temperature of 60 °C for 24 h [33]. The ratio of solid to liquid was 1:50, i.e., each 1 g solid sample was mixed with a 50 mL solution. The water-soluble, ion-exchangeable (mainly organically bound) and acid-soluble inorganic elements were extracted sequentially, and the solid residue implies the HCl insoluble elements, which are mainly present as silicate or aluminosilicate. The solution and digested solid residue were analyzed by Inductively Coupled Plasma Mass Spectrometry (ICP-MS, ELAN DRC-e, PerkinElmer Inc., Hopkinton, MA, USA) to quantitatively determine the amount of inorganic elements. The chemical fractionation of alkali and alkaline earth metals (AAEM) in Zhundong coal is presented in Figure 1. The occurrence form of Na is mostly water-soluble and organically bound, and their total fractions reach nearly 90%. The occurrence forms of Ca and Mg are mostly organically bound and acid-soluble, with total fractions of about 80%. These elements in coal are expected to be the major contributors to inorganic PM, especially for ultrafine particles.

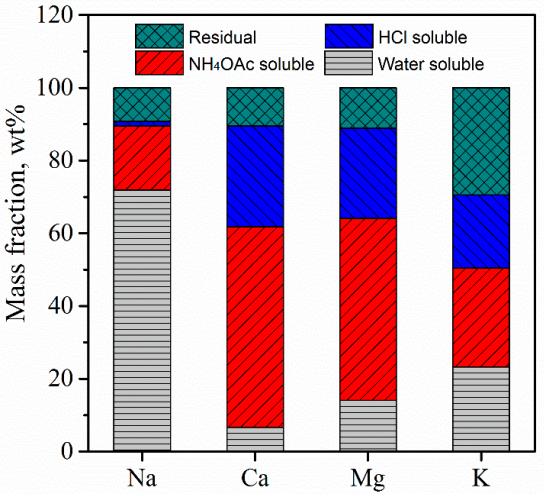

Figure 1. The occurrence form of alkali and alkaline earth metals (AAEM) in Zhundong coal.

Moreover, the Zhundong coal sample was subjected to a CCSEM analysis (Computer-Controlled Scanning Electron Microscopy, GENESIS XM, EDAX Inc., Mahwah, NJ, USA), according to the detailed procedures presented in our prior studies [34,35]. Though it cannot be used to analyze organically bound elements, CCSEM technology is beneficial for determining the types and contents of inorganic minerals and the mass fraction of major elements distributed in those minerals.

2.2. Experimental Setup and Sample Analysis

The coal sample was burned in a well-controlled electrically heated HDTF, as shown in Figure 2. The details of this HDTF can be found in earlier publications [36,37]. The experimental system is composed of four parts: the feeding system; the furnace and temperature controlling system; the gas delivery system and the sampling system. The sampling system consists of a sampling tube, a cyclone, a Dekati low pressure impactor (LPI, Dekati Ltd., Kangasala, Finland) and a vacuum pump. The temperature of the DTF can be adjusted from 1400 °C to 1800 °C with the heating of the molybdenum silicide bars. The length of the reactor tube is 1440 mm, and the inner diameter is 40 mm.

In the experiment, the furnace temperature was controlled at a high temperature of 1500 °C. The combustion experiments of Zhundong coal were carried out at air condition (AIR, O_2/N_2 = 21/79) and at oxy-fuel conditions with three characterized oxygen fractions. The volume ratios of O_2/CO_2 were 21/79 (OXY21), 27/73 (OXY27) and 32/68 (OXY32), respectively. The feeding rate of the coal sample was ~0.15 g/min, the total feeding gas flow rate was 5 L/min and the particle residence time in the furnace was less than 1.5 s. Thermogravimetric analysis (TGA,TGA4000, Perkinelmer Inc, Waltham, MA, USA) confirmed the complete combustion achieved [38], ensuring that all the collections were inorganic PM. After complete combustion, the flue gas containing fine ash was first quenched by N_2, then separated by cyclone with a cutoff of ~10.0 μm and collected by the LPI, which has 13 stages for different size fractions. Stages 1–13 had a D50 size of 0.039, 0.072, 0.122, 0.205, 0.32, 0.488, 0.765, 1.231, 1.951, 3.08, 5.144, 8.099 and 10.747 μm, respectively. In order to avoid acid gas condensation and particle coagulation during sampling, the entire sampling system was externally heated to 120 °C [39].

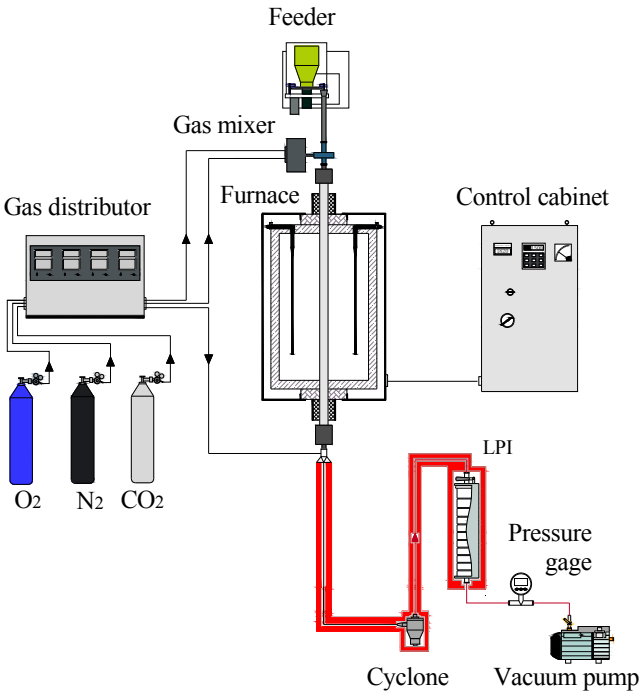

Figure 2. Schematic diagram of high-temperature drop-tube furnace (HDTF).

The mass of aluminum foil in each LPI stage was accurately weighed using a Mettler Toledo Microbalance (readability, 0.001 mg, XS3DU, Mettler Toledo Inc, Zurich, ZH, Switzerland) before and after collection, and was used to determine the mass-based PSDs and mass yields of PM_{10}. The polycarbonate membranes were used for the particle elemental analysis. The elemental compositions of the particles in each stage were analyzed using a scanning electron microscopy (SEM, JSM-6510, JEOL Ltd., Tokyo, Japan) equipped with an energy-dispersive spectrometer (EDS, EDAX GENESIS, EDAX Inc., Mahwah, NJ, USA). At least 3 replicates were performed for each condition, and the reported data and error bar are the mean values.

2.3. Calculation of the Char Particle Combustion Temperature

It is well-known that the O_2 fraction in a combustion atmosphere affects the coal particle combustion temperature [26,30,31]. A simplified single-particle model developed by Jia et al. [30] was used to calculate the char particle combustion temperature during oxy-fuel combustion at different oxygen input fractions. The input char particle size was 80 μm and the input gas temperature was 1773 K (1500 °C). The calculated temperatures for the char particles at different oxygen contents are shown in Table 3. They were 1797 °C for AIR, 1741 °C for OXY21, 1804 °C for OXY27 and 1852 °C for OXY32, respectively.

Table 3. Char particles average burning temperature during oxy-fuel combustion.

Atmosphere	AIR	OXY21	OXY27	OXY32
Char temperature (°C)	1797	1741	1804	1852

3. Results and Discussion

3.1. Particle Size Distributions (PSDs) of Inorganic PM_{10} Generated from Zhundong Coal Combustion

Figure 3 presents the mass-based PSDs of PM_{10} during the air and oxy-fuel combustion of Zhundong coal at three oxygen fractions, which generally display a bimodal distribution of PM_{10}.

The ultrafine particles are centered around 0.1 μm, which were reported to be formed via the vaporization and nucleation of ash species near the burning coal particle firstly and subsequent growth due to the coagulation and/or heterogeneous condensation of inorganic vapors in the cooling flue gas after the boiler [26]. The coarse particles are located at around 5 μm; they are mainly formed through char fragmentation and include mineral coalescence during combustion [40,41].

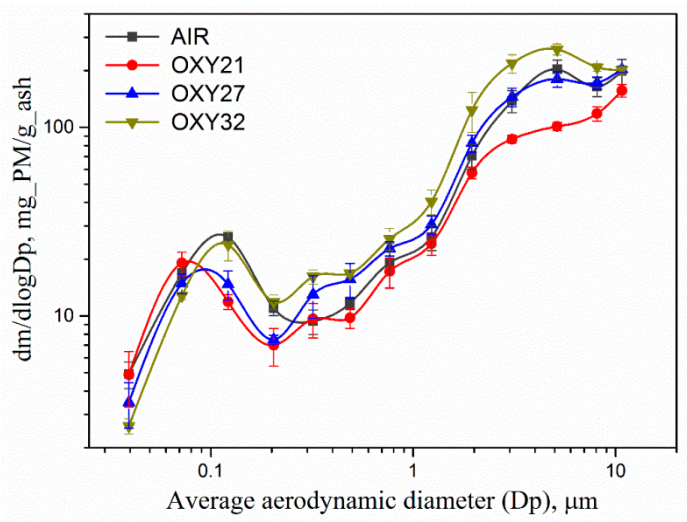

Figure 3. Mass-based particle size distributions (PSDs) of PM_{10} during the air and oxy-fuel combustion of Zhundong coal.

Considering the ultrafine particles, it could be observed that, firstly, the OXY21 condition results in the peak size of the ultrafine mode becoming smaller (about 0.07 μm) compared to the AIR condition, and, secondly, as the oxygen fraction is increased to OXY32 in the O_2/CO_2 mixture, the ultrafine mode center becomes coarser (about 0.1 μm). The phenomena have been identified and explained in earlier studies [25–27]. The low combustion temperature in OXY21 and OXY27 conditions compared to the OXY32 condition should result both in less vaporization and in less particle growth by coagulation, leading to fewer ultrafine particles being formed and the mode center shifting to a smaller size. Moreover, when comparing the OXY27 condition with the AIR condition, which have similar combustion temperatures, an ignition delay can be found during oxy-fuel combustion [42]; the longer reaction time in the AIR condition is beneficial for particle growth by coagulation, causing a larger peak size in the AIR condition than in the OXY27 condition. With regard to the coarse particles (>~0.5 μm), the increased oxygen fraction during O_2/CO_2 combustion significantly increases the char combustion temperature, and promotes both the fragmentation of char particles and the melting and coalescence of the included minerals [26,31], causing a clear tendency of OXY32 > OXY27 > OXY21 for the concentration of coarse particles. The distribution of coarse particles from the AIR condition is very similar to that from the OXY27 condition, as will be discussed in Section 3.4.

3.2. Chemical Compositions of PM_{10}

Figure 4 presents the mass fractions of inorganic elements in PM_{10} from Zhundong coal combustion. Information on the size-dependent chemical composition of PM_{10} has been developed to identify the central mode (i.e., fine fragmentation mode) that exists between the ultrafine and the coarse modes [43]. Figure 4 shows a slight decrease in Na, S and a slightly increase in Ca between ~0.5 μm and 2.5 μm (stages 6–9), implying the typical characteristics of the central mode elaborated by Yu et al. [43]. However, Figure 3 presents the same tendency for OXY32 > OXY27 > OXY21 for the concentration of central mode particles and coarse particles (>2.5 μm), and Figure 4 shows very similar elemental compositions between these two modes for all cases. Therefore, the two mode particles are

analyzed together as $PM_{0.5–10}$ below. As shown in Figure 4, the chemical compositions of $PM_{0.5–10}$ in air and oxy-fuel conditions with different oxygen fractions are very similar; $PM_{0.5–10}$ predominantly contains Ca (~50–65%), and some Mg, S, Al and Si.

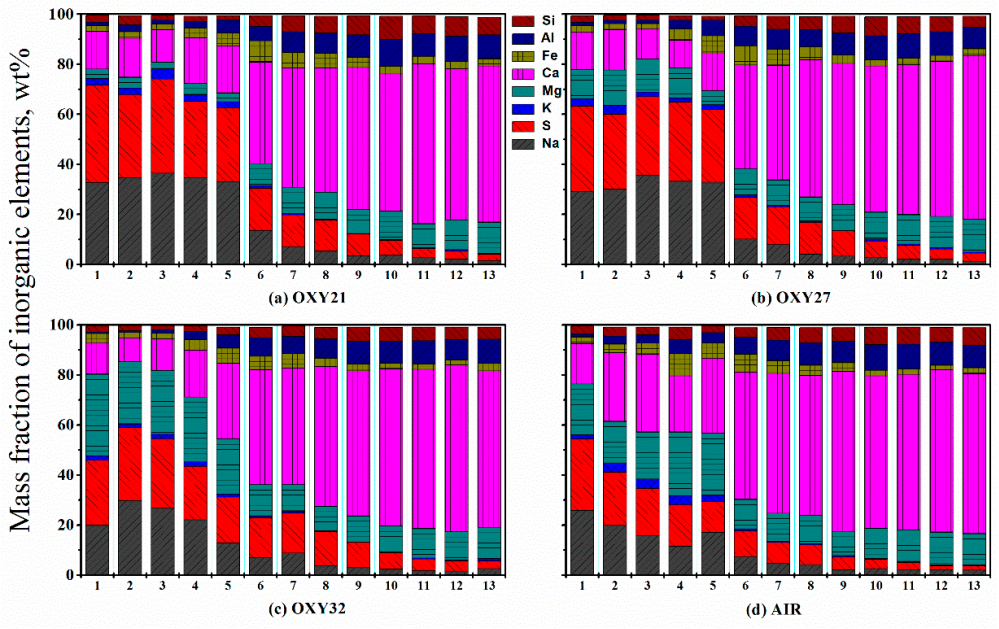

Figure 4. Inorganic elemental composition of PM10 formed during the air and oxy-fuel combustion of Zhundong coal. (**a**) OXY21; (**b**) OXY27; (**c**) OXY32; (**d**) AIR. Stages 1–13 have a D50 size of 0.039, 0.072, 0.122, 0.205, 0.32, 0.488, 0.765, 1.231, 1.951, 3.08, 5.144, 8.099 and 10.747 μm, respectively.

Particles less than 0.5 μm in size (stages 1–5, called ultrafine particles and $PM_{0.5}$) present relatively uniform elemental distributions for each case. $PM_{0.5}$ is composed of Na, S, Mg and Ca, with total fractions of nearly 90%. Comparing air with oxy-fuel conditions, the mass fractions of Ca in $PM_{0.5}$ from the air condition are much higher than those from oxy-fuel conditions, while the fractions of Na and S in $PM_{0.5}$ are obviously lower. Beyond this, as the oxygen concentration increases in oxy-fuel combustion, the mass fractions of Na and S in $PM_{0.5}$ decrease while that of Mg increases distinctly. The phenomena observed will be discussed thoroughly in Section 3.4.

3.3. Mass Yields of PM_{10}

The mass-based yields of $PM_{0.5}$ and $PM_{0.5–10}$ formed during the air and oxy-fuel combustion of Zhundong coal are depicted in Figure 5. Firstly, it can be seen that the yields from OXY32 go up to 200 mg_PM_{10}/g_ash; such a high PM_{10} yield from Zhundong coal compared to other power coals was also found in the study on the air condition by Li et al. [12]. This implies a terrible burden for dust-cleaning apparatuses such as electrostatic precipitators compared to other power coals. Secondly, the promoted O_2 fraction during oxy-fuel combustion increases the PM_{10} yields, especially of $PM_{0.5–10}$, as explained in Section 3.1. Lastly, the yield of $PM_{0.5}$ from AIR is similar to that from OXY32 and higher than that from OXY21 and OXY27, while the yield of $PM_{0.5–10}$ from AIR is lower than that from OXY32 but similar to the OXY27 case. This can be explained by the effect of the combustion atmosphere on the partitioning of major ash-forming inorganic elements.

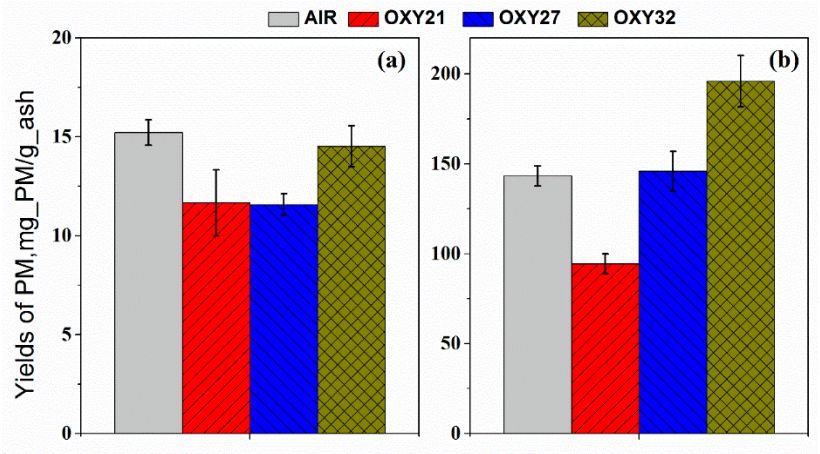

Figure 5. Mass yields of PM_{10} formed during the air and oxy-fuel combustion of Zhundong coal. (**a**) $PM_{0.5}$; (**b**) $PM_{0.5–10}$.

3.4. Influence of Characterized Oxygen Input Fractions on the Emission of $PM_{0.5}$ and $PM_{0.5–10}$

Figure 6 presents the elemental PSDs of PM_{10} while Figure 7 depicts the absolute mass of inorganic elements in $PM_{0.5}$ and $PM_{0.5–10}$, further indicating the mass contribution of various elements to the inorganic $PM_{0.5}$ and $PM_{0.5–10}$. As shown in Figure 6, Si and Al are only enriched in $PM_{0.5–10}$; a weak peak can be noted in $PM_{0.5}$ and an obvious peak in $PM_{0.5–10}$ can be found in PSDs of Mg; as with Ca, Na and S, two obvious peaks occur in both $PM_{0.5}$ and $PM_{0.5–10}$.

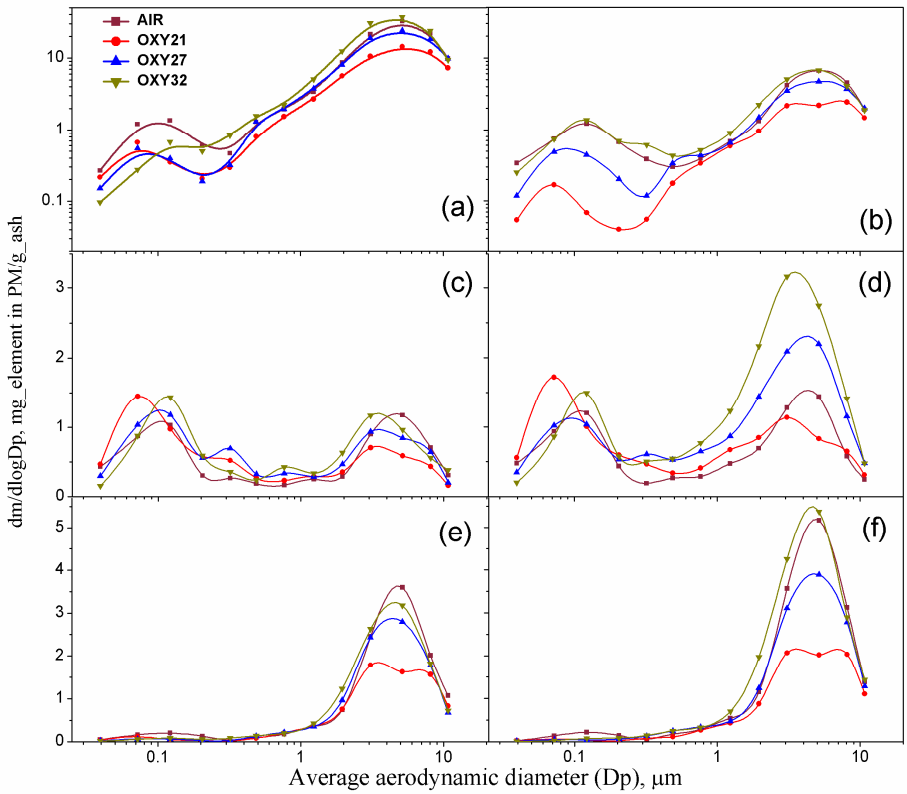

Figure 6. Elemental PSDs of PM_{10} generated from the air and oxy-fuel combustion of ZD coal. (**a**) Ca, (**b**) Mg, (**c**) Na, (**d**) S, (**e**) Si and (**f**) Al.

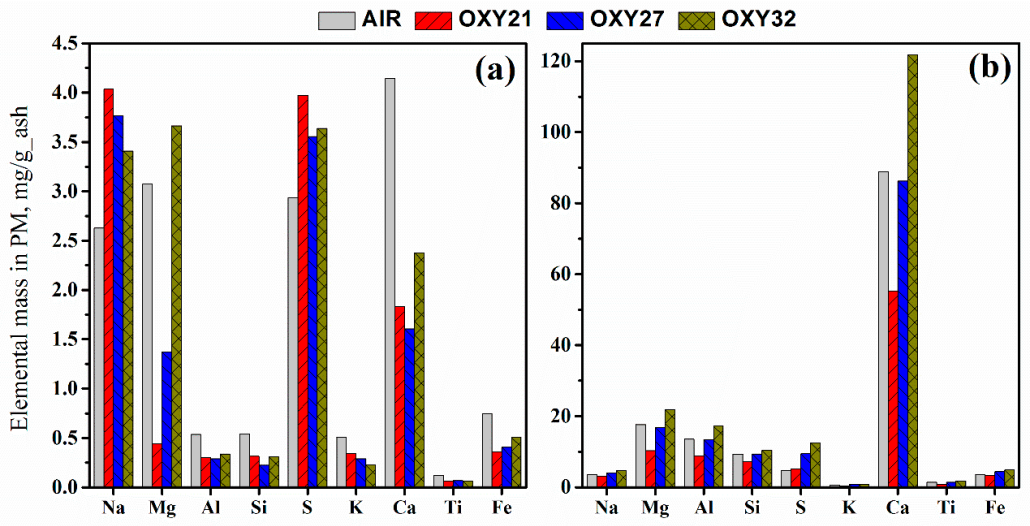

Figure 7. Absolute mass of inorganic elements in (**a**) $PM_{0.5}$ and (**b**) $PM_{0.5–10}$ during air and oxy-fuel combustion.

3.4.1. $PM_{0.5}$

As observed in Figures 6 and 7a, the highest yield of $PM_{0.5}$ from the AIR condition is created mainly by the highest yield of Ca, and the yields of Na and S from AIR are inhibited compared to oxy-fuel combustion. The increased yield of $PM_{0.5,}$ like the increased oxygen fraction during oxy-fuel combustion, is mainly caused by the increase in Mg and Ca (Figure 7a). In Section 3.1, it was noted that the OXY21 condition results in the peak size of the ultrafine mode becoming smaller (about 0.07 μm) compared to the AIR and OXY32 conditions. This is clearly caused by the highest concentrations of Na and S from OXY21 found in Figure 6. The higher content of Na in ultrafine particles generated from lower O_2 fraction of oxy-fuel combustion has also been observed by Kazanc et al. [28].

Partitioning of Ca. Figure 1 shows that more than half of the Ca occurring in Zhundong coal is organically bound, while ~30% of the Ca is HCl-soluble and 10% is residual. The occurrence mode of Mg is similar to Ca. It was noted that 40% of the Ca exists in the inorganic minerals and can be determined by CCSEM, and the data show that ~16% of the Ca in minerals was identified as calcite which is HCl-soluble; the others were identified as complex minerals such as dolomite (Ca-Mg), Ca-Mg-S, part of which should also be HCl-soluble. The last 10% of the residual Ca should exist as aluminosilicates containing Ca, Mg, Fe, Na, etc.

One of the important serial pieces of research on the thermal utilization of Australian low-rank coal by Quyn et al. [44] indicates the reactions of organically bound AAEM during coal combustion as follows:

$$CM\text{-}CH_2\text{-}COOX \rightarrow CM' + CH_3COOX \quad (1)$$

$$CM\text{-}COOX \rightarrow CM\text{-}X + CO_2 \quad (2)$$

$$CM\text{-}X \rightarrow CM + X \quad (3)$$

where X can be Na, K, Mg or Ca, CM and CM′ represent coal or char matrix. Reaction (1) is insensitive to temperature and can take place at relatively low temperatures (e.g., <600 °C). Equation (2) thermally breaks down the carboxylates and releases CO_2. Importantly, reaction (3) is affected by temperature and the bond will be thermally broken at higher temperatures to release AAEM. As a result, the volatilization of organically bound AAEM (e.g., 50% of Ca in Zhundong coal) increases when the char matrix is burned at higher temperatures, generating more ultrafine particles.

The 30% HCl-soluble Ca exists mainly as calcite and dolomite. These minerals undergo decomposition (Equations (4) and (5)), vaporization and fragmentation to form ultrafine particles.

Higher particle-burning temperatures (e.g., AIR and OXY32) and lower CO_2 fractions (e.g., OXY32) promote the reactions.

$$CaCO_3 \rightarrow CaO + CO_2 \quad (4)$$

$$CaCO_3 \cdot MgCO_3 \rightarrow CaO \cdot MgO + 2CO_2 \quad (5)$$

Therefore, the release of Mg and Ca from AIR and OXY32 can be expected to be higher than OXY21 and OXY27, creating higher ultrafine particles (Figure 7a). It should be noted that CO_2 participates in the reactions involving both organically bound Ca (Equation (2)) and calcite (Equation (4)). These reactions found in OXY32 with 68% CO_2 should be inhibited compared to AIR, and a much higher yield of Ca is thus found in $PM_{0.5}$ from AIR combustion.

Partitioning of Na and S. McNallan et al. [45] reported that after coal combustion, most Na is in the form of either NaCl(g) or Na_2SO_4(g), and NaCl will be transferred to Na_2SO_4 when the content of SO_2 in flue gas is high, according to Equation (7).

$$Na_2O + SO_2 + 0.5O_2 \rightarrow Na_2SO_4 \quad (6)$$

$$2NaCl + SO_2 + CO_2 + H_2O \rightarrow Na_2SO_4 + 2HCl + CO \quad (7)$$

Therefore, it is mainly the homogeneous nucleation and heterogeneous condensation of Na_2SO_4 that forms ultrafine particles, as shown in Figure 7a. Figure 1 shows that most Na is water-soluble and organically bound; the vaporization of Na and S can obviously be enhanced by higher combustion temperatures. Biswas et al. [46] have indicated that when the concentration of nascent ultrafine particles is below a critical concentration, the vaporized Na_2SO_4 tends to nucleate, but if the concentration number of nascent particles is higher than the critical number, condensation begins to dominate nucleation. The nucleation of Na_2SO_4 is indeed found to be dominant for OXY21 (Figure 6c,d), forming a higher concentration of particles of less than 0.07 μm and a smaller peak size of the ultrafine mode, as mentioned above (Figure 3). By contrast, with a higher vaporization of Na and S, the condensation of Na_2SO_4 should obviously form larger particles for AIR and OXY32, causing lower concentrations of Na_2SO_4 in $PM_{0.5}$ (Figure 7a).

It has already been noted that the yields of Na and S from AIR are obviously less than those for OXY27 and OXY32. This cannot be explained by the higher vaporization, condensation and growth of Na_2SO_4 considering their comparable particle combustion temperatures. Most of the studies listed in the review by Toftegaard et al. [19] reported a decreased emission of gaseous SOx from oxy-fuel combustion compared to air, because of the higher retention of ash particles for oxy-fuel combustion. This is in line with the higher S contents found in both $PM_{0.5}$ and $PM_{0.5–10}$ from oxy-fuel combustion (Figure 7). More S is thus emitted in gaseous form for AIR, causing the lowest yields in $PM_{0.5}$ observed in Figure 7a. In addition, very high contents of Mg and Ca are reported in $PM_{0.5}$ from AIR, which should serve as a core of submicron particles. This was detected by Neville and Sarofim, who confirmed the core of MgO and Fe in submicron particles of Montana lignite [47]. The most abundant existing core of Mg and Ca for AIR is beneficial for the heterogeneous condensation of Na vapor, therefore a lot of Na grows to $PM_{0.5–10}$ and causes the lowest Na retained in $PM_{0.5}$.

The combination form of major elements in $PM_{0.5}$, i.e., Ca, Na, S and Mg, was also tested. The mole numbers of these elements are depicted in Figure 8. It is noteworthy that the MgO was reported to be inert to the sulfation reaction, and $MgSO_4$ is thermodynamically unfavorable at a temperature of >800 °C [48], therefore Mg should serve as a core of ultrafine particles and shows little reaction with S. It can also be observed in Figure 8 that the mole number of S is almost equal to the sum of Ca and Na during oxy-fuel combustion. This shows that during oxy-fuel combustion, the occurrence forms of sulfur in $PM_{0.5}$ are mostly Na_2SO_4 and $CaSO_4$, and more Ca is found in OXY32 which should serve as a CaO core. For the AIR condition, the highest Ca as well as the lowest Na and S in $PM_{0.5}$ shown in Figure 7a imply that more Ca exists as the inner core of ultrafine particles correspondingly.

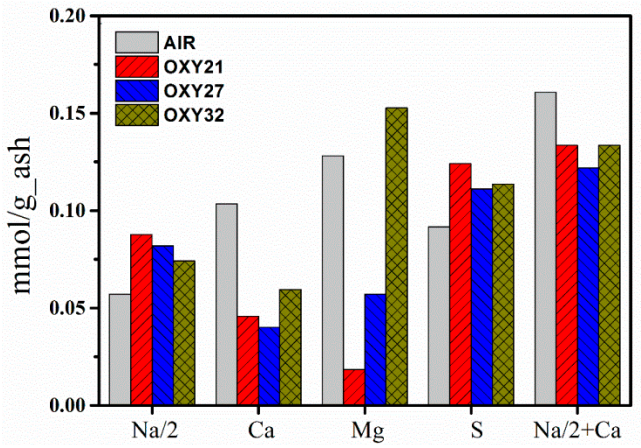

Figure 8. Mole numbers of major inorganic elements in $PM_{0.5}$ during air and oxy-fuel combustion.

3.4.2. $PM_{0.5–10}$

The very similar yields of various elements except S in $PM_{0.5–10}$ from AIR and OXY27 are found in Figure 7b, supporting the similar yield of AIR as OXY27 shown in Figure 5b. Because there is no apparent impact on the partitioning of individual elements, the nearly identical particle-burning temperature between AIR and OXY27 (Table 3) should be responsible for their similar $PM_{0.5–10}$ yields. It is noteworthy that the slightly lower amount of Ca in OXY27 is caused by Equations (2) and (4), which inhibits the transformation of Ca, while the higher content of S in OXY27 can be attributed to the above-mentioned retention of ash particles in oxy-fuel combustion.

Figures 6 and 7b also show that the absolute mass of various inorganic elements in $PM_{0.5–10}$ increases with the increased oxygen fraction during oxy-fuel combustion, especially for Ca, which leads to an obvious increase in the $PM_{0.5–10}$ yield. The irrelevance with the individual elemental yield reveals that both the fragmentation of char particles and the melting and coalescence of the included minerals are increased by higher char combustion temperatures [31,33]. The extensive fragmentation of low-rank coal even in the ignition stage has already been observed by Khatami et al. [42].

4. Conclusions

In this paper, Zhundong sub-bituminous coal was combusted in a high-temperature DTF, and the emission behaviors of inorganic PM_{10} during air and oxy-fuel combustion at three characterized oxygen fractions comparable to air combustion were studied in detail. The results are as follows:

(1) The emission yield of Zhundong coal is very high and reaches up to 200 mg_PM_{10}/g_ash. It is much higher than other power coal and must be a terrible burden for dust-cleaning apparatuses.

(2) In all cases, inorganic $PM_{0.5}$ is composed of Na, S, Mg and Ca, with total fractions of ~90%, while $PM_{0.5–10}$ predominantly contains Ca (~50–65%), and some Mg, S, Al and Si.

(3) At three characterized oxygen fractions during oxy-fuel combustion (OXY21, 27 and 32), the promoted O_2 fraction increases the yields of both $PM_{0.5}$ and $PM_{0.5–10}$. Higher particle-burning temperatures and lower CO_2 fractions promote the reactions of both organically bound elements and minerals, increasing the partitioning of Mg and Ca, and causing an increased yield of $PM_{0.5}$. The fragmentation of char particles and the melting and coalescence of the included minerals are increased by the higher char combustion temperature to form more $PM_{0.5–10}$.

(4) The yield of $PM_{0.5}$ from AIR is high and similar to that from OXY32 while the yield of $PM_{0.5–10}$ from AIR is similar to the OXY27 case. The high yield of $PM_{0.5}$ from AIR is mainly caused by the highest yield of Ca in four conditions. The very similar particle-burning temperature of AIR and OXY27 should be responsible for their similar $PM_{0.5–10}$ yields as there is no apparent impact on the partitioning of individual elements.

Author Contributions: B.F. performed the experiments, analyzed the data, and wrote the paper; C.W. supervised this project, designed the experiments, and revised the paper; X.Z., J.W. and X.Y. helped with the experiments.

Funding: This research was funded by the National Nature Science Foundation of China (No. 51520105008, 51661125011, 51506067).

Acknowledgments: The authors like to acknowledge the Analytical and Testing Center at the Huazhong University of Science and Technology for the ICP-MS and XRF testing of samples.

Conflicts of Interest: The authors declare no conflict of interest.

References

1. You, C.; Xu, X. Coal combustion and its pollution control in China. *Energy* **2010**, *35*, 4467–4472. [CrossRef]
2. Xu, M.; Yu, D.; Yao, H.; Liu, X.; Qiao, Y. Coal combustion-generated aerosols: Formation and properties. *Proc. Combust. Inst.* **2011**, *33*, 1681–1697. [CrossRef]
3. Xu, M.; Qiao, Y.; Zheng, C.; Li, L.; Liu, J. Modeling of homogeneous mercury speciation using detailed chemical kinetics. *Combust. Flame* **2003**, *132*, 208–218. [CrossRef]
4. Luo, G.; Yao, H.; Xu, M.; Gupta, R.; Xu, Z. Identifying modes of occurrence of mercury in coal by temperature programmed pyrolysis. *Proc. Combust. Inst.* **2011**, *33*, 2763–2769. [CrossRef]
5. Wen, C.; Gao, X.; Yun, Y.; Wu, J.; Xu, M.; Wu, H. Emission of inorganic PM_{10} from included mineral matter during the combustion of pulverized coals of various ranks. *Fuel* **2015**, *140*, 526–530. [CrossRef]
6. Lei, M.; Sun, C.; Wang, C. Techno-Economic Analysis of a 600 MW oxy-Enrich pulverized coal-Fired boiler. *Energies* **2018**, *11*, 768. [CrossRef]
7. Zhang, Z.; Zhu, M.; Li, J.; Zhang, K.; Xu, G.; Zhang, D. Experimental study of ignition and combustion characteristics of single particles of Zhundong lignite. *Energy Fuels* **2017**, *32*, 4221–4226. [CrossRef]
8. Kazagic, A.; Hodzic, N.; Metovic, S. Co-combustion of low-rank coal with woody biomass and miscanthus: An experimental study. *Energies* **2018**, *11*, 601. [CrossRef]
9. Khatami, R.; Levendis, Y.A. An overview of coal rank influence on ignition and combustion phenomena at the particle level. *Combust. Flame* **2016**, *164*, 22–34. [CrossRef]
10. Torresi, M.; Fornarelli, F.; Fortunato, B.; Camporeale, S.; Saponaro, A. Assessment against experiments of devolatilization and char burnout models for the simulation of an aerodynamically staged swirled low-NOx pulverized coal burner. *Energies* **2017**, *10*, 66. [CrossRef]
11. Wang, X.; Xu, Z.; Wei, B.; Zhang, L.; Tan, H.; Yang, T.; Mikulčić, H.; Duić, N. The ash deposition mechanism in boilers burning Zhundong coal with high contents of sodium and calcium: A study from ash evaporating to condensing. *Appl. Therm. Eng.* **2015**, *80*, 150–159. [CrossRef]
12. Li, G.; Li, S.; Huang, Q.; Yao, Q. Fine particulate formation and ash deposition during pulverized coal combustion of high-sodium lignite in a down-fired furnace. *Fuel* **2015**, *143*, 430–437. [CrossRef]
13. Wu, X.; Zhang, X.; Yan, K.; Chen, N.; Zhang, J.; Xu, X.; Dai, B.; Zhang, J.; Zhang, L. Ash deposition and slagging behavior of Chinese Xinjiang high-alkali coal in 3 MW th pilot-scale combustion test. *Fuel* **2016**, *181*, 1191–1202. [CrossRef]
14. Zhou, B.; Zhou, H.; Wang, J.; Cen, K. Effect of temperature on the sintering behavior of Zhundong coal ash in oxy-fuel combustion atmosphere. *Fuel* **2015**, *150*, 526–537. [CrossRef]
15. Li, J.; Zhu, M.; Zhang, Z.; Kai, Z.; Shen, G.; Zhang, D. Characterisation of ash deposits on a probe at different temperatures during combustion of a Zhundong lignite in a drop-tube furnace. *Fuel Process. Technol.* **2016**, *144*, 155–163. [CrossRef]
16. Xu, J.; Yu, D.; Fan, B.; Zeng, X.; Lv, W.; Chen, J. Characterization of ash particles from co-combustion with a Zhundong coal for understanding ash deposition behavior. *Energy Fuels* **2012**, *28*, 678–684. [CrossRef]
17. Fuller, A.; Maier, J.; Karampinis, E.; Kalivodova, J.; Grammelis, P.; Kakaras, E.; Scheffknecht, G.; Sciubba, E. Fly Ash formation and characteristics from (co-)combustion of an herbaceous biomass and a Greek lignite (low-rank coal) in a pulverized fuel pilot-Scale test facility. *Energies* **2018**, *11*, 1581. [CrossRef]
18. Buhre, B.J.P.; Elliott, L.K.; Sheng, C.; Gupta, R.P.; Wall, T.F. Oxy-fuel combustion technology for coal-fired power generation. *Prog. Energy Combust. Sci.* **2005**, *31*, 283–307. [CrossRef]
19. Toftegaard, M.B.; Brix, J.; Jensen, P.A.; Glarborg, P.; Jensen, A.D. Oxy-fuel combustion of solid fuels. *Prog. Energy Combust. Sci.* **2010**, *36*, 581–625. [CrossRef]

20. Lei, K.; Ye, B.; Cao, J.; Zhang, R.; Liu, D. Combustion characteristics of single particles from bituminous coal and pine sawdust in O_2/N_2, O_2/CO_2, and O_2/H_2O atmospheres. *Energies* **2017**, *10*, 1695. [CrossRef]
21. Guo, J.; Liu, Z.; Huang, X.; Zhang, T.; Luo, W.; Hu, F.; Li, P.; Zheng, C. Experimental and numerical investigations on oxy-coal combustion in a 35 MW large pilot boiler. *Fuel* **2017**, *187*, 315–327. [CrossRef]
22. Molina, A.; Shaddix, C.R. Ignition and devolatilization of pulverized bituminous coal particles during oxygen/carbon dioxide coal combustion. *Proc. Combust. Inst.* **2007**, *31*, 1905–1912. [CrossRef]
23. Yu, D.; Morris, W.J.; Erickson, R.; Wendt, J.O.L.; Fry, A.; Senior, C.L. Ash and deposit formation from oxy-coal combustion in a 100 kW test furnace. *Int. J. Greenh. Gas Control* **2011**, *5*, S159–S167. [CrossRef]
24. Morris, W.J.; Yu, D.; Wendt, J.O.L. Soot, unburned carbon and ultrafine particle emissions from air and oxy-coal flames. *Proc. Combust. Inst.* **2011**, *33*, 3415–3421. [CrossRef]
25. Suriyawong, A.; Gamble, M.; Lee, M.; Axelbaum, R.A.; Biswas, P. Submicrometer particle formation and mercury speciation under O_2-CO_2 coal combustion. *Energy Fuels* **2006**, *20*, 2357–2363. [CrossRef]
26. Sheng, C.; Li, Y.; Liu, X.; Yao, H.; Xu, M. Ash particle formation during O_2/CO_2 combustion of pulverized coals. *Fuel Process. Technol.* **2007**, *88*, 1021–1028. [CrossRef]
27. Sheng, C.; Li, Y. Experimental study of ash formation during pulverized coal combustion in O_2/CO_2 mixtures. *Fuel* **2008**, *87*, 1297–1305. [CrossRef]
28. Kazanc, F.; Levendis, Y.A. Physical properties of particulate matter emitted from combustion of coals of various ranks in O_2/N_2 and O_2/CO_2 environments. *Energy Fuels* **2012**, *26*, 7127–7139. [CrossRef]
29. Kazanc, F.; Levendis, Y.A.; Maffei, T. Chemical composition of submicrometer particulate matter (PM_1) emitted from combustion of coals of various ranks in O_2/N_2 and O_2/CO_2 environments. *Energy Fuels* **2013**, *27*, 4984–4998. [CrossRef]
30. Jia, Y.; Lighty, J.S. Ash particulate formation from pulverized coal under oxy-fuel combustion conditions. *Environ. Sci. Technol.* **2012**, *46*, 5214–5221. [CrossRef] [PubMed]
31. Liu, X.; Xu, M.; Hong, Y.; Yu, D.; Gao, X.; Cao, Q.; Cai, Y. Effect of combustion parameters on the emission and chemical composition of particulate matter during coal combustion. *Energy Fuels* **2007**, *21*, 157–162. [CrossRef]
32. Zeng, X.; Yu, D.; Liu, F.; Fan, B.; Wen, C.; Yu, X.; Xu, M. Scavenging of refractory elements (Ca, Mg, Fe) by kaolin during low rank coal combustion. *Fuel* **2018**, *223*, 198–210. [CrossRef]
33. Wang, C.; Jin, X.; Wang, Y.; Yan, Y.; Cui, J.; Liu, Y.; Che, D. Release and transformation of sodium during pyrolysis of Zhundong coals. *Energy Fuels* **2015**, *29*, 78–85. [CrossRef]
34. Wen, C.; Xu, M.; Zhou, K.; Yu, D.; Zhan, Z.; Mo, X. The melting potential of various ash components generated from coal combustion: Indicated by the circularity of individual particles using CCSEM technology. *Fuel Process. Technol.* **2015**, *133*, 128–136. [CrossRef]
35. Wen, C.; Gao, X.; Xu, M. A CCSEM study on the transformation of included and excluded minerals during coal devolatilization and char combustion. *Fuel* **2016**, *172*, 96–104. [CrossRef]
36. Wang, C.; Liu, X.; Li, D.; Wu, W.; Xu, Y.; Si, J.; Zhao, B.; Xu, M. Effect of H_2O and SO_2 on the distribution characteristics of trace elements in particulate matter at high temperature under oxy-fuel combustion. *Int. J. Greenh. Gas Control* **2014**, *23*, 51–60. [CrossRef]
37. Wen, C.; Zhang, P.; Yu, D.; Gao, X.; Xu, M. Loading identical contents of sodium and quartz into different ash-removed coals to elaborately investigate the real effects of coal particle combustion on the emission behavior of PM_{10}. *Proc. Combust. Inst.* **2017**, *36*, 2191–2198. [CrossRef]
38. Gao, X.; Rahim, M.U.; Chen, X.; Wu, H. Inorganic PM_{10} emission from the combustion of individual mallee components and whole-tree biomass. *Proc. Combust. Inst.* **2017**, *36*, 3313–3319. [CrossRef]
39. Gao, X.; Wu, H. Effect of sampling temperature on the properties of inorganic particulate matter collected from biomass combustion in a drop-tube furnace. *Energy Fuels* **2010**, *24*, 4571–4580. [CrossRef]
40. Wen, C.; Xu, M.; Yu, D.; Sheng, C.; Wu, H.; Zhang, P.A.; Qiao, Y.; Yao, H. PM_{10} formation during the combustion of N_2-char and CO_2-char of Chinese coals. *Proc. Combust. Inst.* **2013**, *34*, 2383–2392. [CrossRef]
41. Sheng, C. Char structure characterised by Raman spectroscopy and its correlations with combustion reactivity. *Fuel* **2007**, *86*, 2316–2324. [CrossRef]
42. Khatami, R.; Stivers, C.; Joshi, K. Combustion behavior of single particles from three different coal ranks and from sugar cane bagasse in O_2/N_2 and O_2/CO_2 atmospheres. *Combust. Flame* **2012**, *159*, 1253–1271. [CrossRef]

43. Yu, D.; Xu, M.; Yao, H.; Sui, J.; Liu, X.; Yu, Y.; Cao, Q. Use of elemental size distributions in identifying particle formation modes. *Proc. Combust. Inst.* **2007**, *31*, 1921–1928. [CrossRef]
44. Quyn, D.M.; Wu, H.; Li, C.Z. Volatilisation and catalytic effects of alkali and alkaline earth metallic species during the pyrolysis and gasification of Victorian brown coal. Part I. Volatilisation of Na and Cl from a set of NaCl-loaded samples. *Fuel* **2002**, *81*, 143–149. [CrossRef]
45. Mcnallan, M.J.; Yurek, G.J.; Elliott, J.F. The formation of inorganic particulates by homogeneous nucleation in gases produced by the combustion of coal. *Combust. Flame* **1981**, *42*, 45–60. [CrossRef]
46. Biswas, P.; Wu, C.Y. Control of toxic metal emissions from combustors using sorbents: A review. *J. Air Waste Manag. Assoc.* **1998**, *48*, 113–127. [CrossRef] [PubMed]
47. Neville, M.; Sarofim, A.F. The stratified composition of inorganic submicron particles produced during coal combustion. *Symp. (Int.) Combust.* **1982**, *19*, 1441–1449. [CrossRef]
48. Fuertes, A.B.; Velasco, G.; Alvarez, T.; Fernandez, M.J. Sulfation of dolomite particles at high CO_2 partial pressures. *Thermochim. Acta* **1995**, *254*, 63–78. [CrossRef]